

J. Environ. Treat. Tech. ISSN: 2309-1185

Journal web link: http://www.jett.dormaj.com



# CFD Modeling of Polypropylene Fluidized Bed Reactor

Hossein Esmaeili<sup>1\*</sup>, Salar Azizi<sup>1</sup>, Seyyed Mojtaba Mousavi<sup>2</sup>, Seyyed Alireza Hashemi<sup>2</sup>

<sup>1</sup>Department of Chemical Engineering, Bushehr Branch, Islamic Azad University, Bushehr, Iran <sup>2</sup>Department of Medical Nanotechnology, School of Advanced Medical Sciences and Technologies, Shiraz University of Medical Sciences, Shiraz, Iran

#### **Abstract**

Poly propylene is one of the famous polymers with great application. In this study, CFD model on dynamics of the fluidized bed polyethylene production process has been investigated. A detailed CFD model for sticky poly propylene fluidized bed was formulated in this work. As a result, detailed information on the PSD and hydrodynamic fields of the gas and solid phases can be obtained from the simulations. Defluidization due to particle aggregation also can be simulated. For modeling plant-scale poly propylene reactors, a chemical look-up table should be used to solve efficiently the solid species equations. In order to address all the issues in FB polymerization, models for simplified polymerization kinetics, polydisperse multiphase flow, and mass and heat transfer between the gas and solid particles are combined together. As a result, physically aggregation because of a tactic polypropylene is more important than other aggregation reasons. Finally, as mentioned earlier, after DQMOM is applied to the multi-fluid CFD model, new terms accounting for the effect of aggregation and breakage need to be added on the right-hand sides of the solid-phase momentum, energy, and species equations.

Keywords: Polypropylene, Reactor, Fluidized bed, Kinetic theory, CFD

#### 1 Introduction

Poly propylene (PP) is one of the famous polymers with great application. Recent PP production reactor technology is a gas-phase fluidized bed and stirred bed. In gas-phase polymerization, small particles (e.g., 20-80 µm) are introduced at a point above the gas distributor, and when exposed to the gas flow containing the monomer, polymerization occurs (1-3). At the early stage of polymerization, the catalyst particles fragment into a large number of small particles, which are quickly encapsulated by the newly-formed polymer and grow continuously, reaching a typical size of 200-3000 µm. Due to the differences in the polymer particle size, segregation occurs and fully-grown polymer particles migrate to the bottom where they are removed from the reactor. The smaller pre-polymerized particles and fresh catalyst particles tend to migrate to the upper portions of the reactor and continue to react with monomers. Because polymerization is exothermic, the temperature of polymer tend to rise and sometimes it will exceed the melting point of the polymer, then polymer particle can become sticky and during collisions can form large agglomerates that can possibly undergo sintering and cause defluidization. In the opposite situation, if the bed is too cold, the particles can become brittle and may fracture forming unwanted small fragments that elutriate with the gas. Hence, heat and mass transfer to particle surface controls the local particle temperature and the rate of agglomeration and breakage (4).

At PP polymerization reactors, propylene as a monomer contact with Ziegler-Natta catalyst which activated with co catalyst and forms poly propylene. PP collected to three types as isotactic, atactic and syndiotactic. Purpose is isotactic PP production and avoids great amount atactic PP production. Atactic poly propylene percentage specification is by means xylene solubility percentage. Atactic PP is liquefied and a small percentage of its made special application of PP, but a great amount of atactic PP make sticky powder and ultimately cause choking bed and effect to PSD at PP polymerization reactor. A stereo modifier as an external donor used to avoid unwanted xylene solubility of PP. donor usage is small as a catalyst. Partially a special Ziegler-Natta catalyst used with the internal donor. Normally industrial PP reactors haven't syndiotactic PP production. In this paper, a cold PP gas fluidized bed when PP powder is sticky (xylene solubility is upper) studied which could give valuable information about this matter and help to design, optimization and scale up with avoiding choking.

#### 2 Modeling equations

Two methods improved for CFD modeling of gas-solid flows, discrete element model (DEM) and two fluid model (TFM). In the DEM gas phase is described by locally averaged Navier-Stokes equations. Newtonian equations of motion for individual particles are then solved and individual particle trajectories are traced, taking into account effects of particle collisions and forces acting on the particle by flowing gas. In such models, the computational demand rises strongly with the number of traced particles, which limits its applicability. In the TFM model, based on the momentum, two phases are mathematically treated as interpenetrating continua. The success of TFM depends on the proper description of the interfacial forces and the solid stress. The interfacial forces are used to describe the momentum transfer

between the two phases which has the primary effect on the hydrodynamic behavior. The stress which represents the solid phase force due to particle-particle interactions has only secondary effect. By introducing the concepts of solid "pressure" and "viscosity", the well-known granular kinetic theory has been employed for computation of the solid stress. In the TFM models, the conservation equations for each of the two phases are derived to obtain a set of the equation with the similar mathematical structure for both phases, which makes the mathematical manipulation of the system relatively easier and minimizes the computation cost (5, 6).

Governing equations detailed for more reliability. Conservation equations and related terms have shown in this section. Meanings of the symbols used are listed in the Nomenclature section.

#### 2.1 Conservation of Mass

The continuity equation for the gas phase is (7, 8):

$$\frac{\partial}{\partial t} \left( \varepsilon_g \rho_g \right) + \nabla \cdot \left( \varepsilon_g \rho_g V_g \right) = \sum_{n=1}^{N_{gn}} R_{gn} \tag{1}$$

There are M solids-phase continuity equations as follows:

$$\frac{\partial}{\partial t} (\varepsilon_{sm} \rho_{sm}) + \nabla \cdot (\varepsilon_{sm} \rho_{sm} \bar{V}_{sm}) = \sum_{n=1}^{N_{sm}} R_{smn}$$
 (2)

The first term on the left in equations (1) and (2) accounts for the rate of mass accumulation per unit volume, and the second term is the net rate of convective mass flux. The term on the right accounts for inters phase mass transfer because of chemical reactions or physical processes, such as evaporation.

#### 2.2 Granular energy conservation

The kinetic theory describing the flow of smooth, slightly inelastic, spherical particles were used in the derivation of the constitutive relation describing the stress tensor in the  $m^{th}$  solids phase,  $\overline{S}_{sm}$ . The resulting constitutive relations contain the quantity  $\Theta_m$ , called the Granular temperature of the  $m^{th}$  solids phase. The granular temperature is proportional to the granular energy of the continuum, where granular energy is defined as the specific kinetic energy of the random fluctuating component of the particle velocity:

$$\Theta_m = \frac{1}{3} < C_m^2 > \tag{3}$$

Where  $<\overrightarrow{C_m}>$  is the fluctuating component of the instantaneous velocity  $\overrightarrow{V}_{sm}$  of the  $m^{th}$  solids phase defined by:

$$\bar{c}_m = \bar{V}_{sm} + \bar{C}_m \tag{4}$$

The transport of granular energy in the m<sup>th</sup> solids phase is governed by following equation:

$$\frac{3}{2} \frac{\partial}{\partial t} \alpha_{sm} \rho_{sm} \Theta_m + \frac{3}{2} \nabla \cdot \alpha_{sm} \rho_{sm} \Theta_m \overrightarrow{V}_{sm} 
= \left[ \overline{S}_{sm} : \nabla \overrightarrow{V}_{sm} - \nabla \cdot \overrightarrow{q}_{\Theta_m} - \gamma_{\Theta_m} + \varphi_{gm} \right] 
+ \sum_{\substack{l=1\\l\neq m}}^{M} \varphi_{lm} .$$
(5)

Where,  $\gamma_{\theta_m}$  is the rate of granular energy dissipation due to inelastic collisions and  $q_{\theta_m}$  is the diffusive flux of granular energy. The term  $\varphi_{gm}$  accounts for the transfer of granular energy between the gas phase and the m<sup>th</sup> solids phase, whereas  $\varphi_{lm}$  accounts for the transfer of granular energy between the m<sup>th</sup> and l<sup>mt</sup> solids phases. Supplying constitutive relations for granular energy equation and numerically solving the M coupled partial differential equations it represents is an onerous task.

The granular energy equation is still under development. An algebraic expression for granular temperature,  $\Theta_m$ , obtained from the energy equation of Lun (9), by assuming that the granular energy is dissipated locally; neglecting the convection and diffusion contributions; and retaining only the generation and dissipation terms (10-12). The resulting algebraic granular energy equation is:

$$\begin{split} &\theta_{m} \\ &= \left[ \frac{-K_{1m}\alpha_{sm}tr(\overline{D}_{sm})}{2\alpha_{sm}K_{4m}} \right. \\ &\left. + \frac{\sqrt{K_{1m}^{2}tr^{2}(\overline{D}_{sm})\alpha_{sm}^{2} + 4K_{4m}\alpha_{sm}\left(K_{2m}tr^{2}(\overline{D}_{sm}) + 2K_{3m}tr(\overline{D}_{sm}^{2})\right)}}{2\alpha_{sm}K_{4m}} \right]^{2} \\ &\left. K_{4m} = \frac{12(1 - e_{mm}^{2})\rho_{sm}g_{0mm}}{d_{mm}\sqrt{\pi}} \end{split} \tag{7}$$

#### 2.3 Conservation of Momentum

The gas-phase momentum balance is expressed as (7, 8):

$$\begin{split} \frac{\partial}{\partial t} \left( \varepsilon_g \rho_g \, \overrightarrow{V}_g \right) + \nabla \cdot \left( \varepsilon_g \rho_g \, \overrightarrow{V}_g \, \overrightarrow{V}_g \right) \\ &= \nabla \cdot \overrightarrow{S}_g + \varepsilon_g \rho_g \, \overrightarrow{g} - \sum_{j=1}^M \overrightarrow{I}_{gm} + \overrightarrow{f}_g \end{split} \tag{8}$$

where  $\overline{S_g}$  is the gas-phase stress tensor,  $\overrightarrow{I_{gm}}$  is an interaction force representing the momentum transfer between the gas phase and the m solids phase, and is the flow resistance offered by internal porous surfaces. The momentum equation for the m solids phase is

$$\frac{\partial}{\partial t} \left( \varepsilon_{sm} \rho_{sm} \overrightarrow{V_{sm}} \right) + \nabla \cdot \left( \varepsilon_{sm} \rho_{sm} \overrightarrow{V_{sm}} \overrightarrow{V_{sm}} \right) \\
= \nabla \cdot \overrightarrow{S_{sm}} + \varepsilon_{sm} \rho_{sm} \overrightarrow{g} + \overrightarrow{I_{gm}} \\
- \sum_{l=1}^{M} \overrightarrow{I_{ml}} \tag{9}$$

Where  $\overline{S_{sm}}$  is the stress tensor for the m solids phase. The term  $\overrightarrow{I_{mt}}$  is the interaction force between the m and 1 solids phases. The first term on the left in these momentum equations represents the net rate of momentum increase. The second term on the left represents the net rate of momentum transfer by convection. The first term on the right represents normal and shear surface forces, while the second term represents body forces (gravity in this case). The next term in equation (8) represents the momentum transfer between the fluid and solids phases; the final term represents the momentum transfer between the fluid and a rigid porous structure. The last two terms in equation (9) represent the momentum exchange between the fluid and solids phases and between the different solids phases, from left to right.

#### 2.3.1 Fluid-Solids Momentum Transfer

The interaction force, or momentum transfer between the gas and the  $\alpha^{th}$  solid phase, is modeled by:

$$\overrightarrow{I_{gm}} = -\varepsilon_{sm} \nabla P_g - F_{gm} \left( \overrightarrow{V_{sm}} - \overrightarrow{V_g} \right) \tag{10}$$

Where the first term on right side describes the buoyancy force, the second term describes the drag force.

Syamlal and O'Brien (1987) derived the following formula for converting terminal velocity correlations to drag correlations (13):

$$F_{gm} = \frac{3\varepsilon_{sm}\varepsilon_{g}\rho_{g}}{4V_{rm}^{2}d_{nm}}C_{Ds}\left(\frac{Re_{m}}{V_{rm}}\right)\left|\overrightarrow{V_{sm}} - \overrightarrow{V_{g}}\right| \tag{11}$$

Where Vrm is the terminal velocity correlation for the mth solids phase. Vrm can be calculated from the Richardson (1954) (14), correlation only numerically; an explicit formula cannot be derived. However, a closed formula for  $V_{rm}$  can be derived from a similar correlation developed by Garside (15),

$$V_{rm} = 0.5(A - 0.06 Re_m + \sqrt{(0.06Re_m)^2 + 0.12 Re_m(2B - A) + A^2})$$
 (12)

$$A = \varepsilon_g^{4.14} \& B$$

$$= \begin{cases} 0.8\varepsilon_g^{1.28} & if & \varepsilon_g \le 0.85 \\ \varepsilon_g^{2.65} & if & \varepsilon_g > 0.85 \end{cases}$$
(13)

And the Reynolds number of the  $m^{th}$  solids phase is given by

$$Re_m = \frac{d_{pm}|\bar{V}_{sm} - \bar{V}_g|\rho_g}{\mu_g} \tag{14}$$

Here,  $C_{Ds}$  ( $Re_m/V_{rm}$ ) is the single-sphere drag function. Of the numerous expressions available for  $C_{Ds}$  (16), we chose the following simple formula proposed by Dalla Valle (17):

$$C_{DS}(Re) = \left(0.63 + \frac{4.8}{\sqrt{Re}}\right)^2$$
 (15)

To use this formula in equation (8), note that Re must be replaced with Rem/Vrm.

#### 2.3.2 Solids-Solids Momentum Transfer

Compared to fluid-solids momentum transfer, much less is known about solids-solids momentum transfer. It is safe to assume that the major effect is the drag between the phases because of velocity differences. Arastoopour (18), observed that such a term is necessary to correctly predict segregation among particles of different sizes in a pneumatic conveyor. Arastoopour (19) studied this effect experimentally in a pneumatic conveyor. Equations to describe such interactions have been derived or suggested by several researchers: Soo (20), Nakamura (21), Syamlal (10, 22), and Srinivasan (23). In the present work the solids-solids momentum transfer,  $I_{\rm ml}$ , is represented as

$$\overrightarrow{I_{ml}} = -F_{sml} \left( \overrightarrow{V_{sl}} - \overrightarrow{V_{sm}} \right) \tag{16}$$

A simplified version of the kinetic theory was used by Syamlal [7], to derive an expression for the drag coefficient Fsml

$$A = 3(1 + e_{lm})(\pi/2 + C_{flm}\pi^2/8)\varepsilon_{sl}\rho_{sl}\varepsilon_{sm}\rho_{sm}$$
 (17-a)

$$F_{sml} = \frac{A(d_{pl} + d_{pm})^2 g_{0lm} \left| \overrightarrow{V_{sl}} - \overrightarrow{V_{sm}} \right|}{2\pi (\rho_{sl} d_{pl}^3 + \rho_{sm} d_{pm}^3)}$$
(17b)

Where elm and  $C_{\rm flm}$  are the coefficient of restitution and coefficient of friction, respectively, between the  $l^{th}$  and  $m^{th}$  solids-phase particles. The radial distribution function at contact  $g_{0_{lm}}$  is that derived by Lebowitz (24) for a mixture of hard spheres:

$$g_{0_{lm}} = \frac{1}{\varepsilon_g} + \frac{3d_{pl}d_{pm}}{\varepsilon_g^2(d_{pl} + d_{pm})} \sum_{l=1}^M \frac{\varepsilon_{s\lambda}}{d_{p\lambda}}$$
 (18)

#### 2.3.3 Fluid-Phase Stress Tensor

The stress tensor for the fluid phase, either gas or liquid, is given by:

$$\bar{\bar{S}}_q = -P_q \bar{\bar{I}} + \bar{\bar{\tau}}_q \tag{19}$$

Where Pg is the pressure. The viscous stress tensor,  $g\tau$ , is assumed to be of the Newtonian form.

$$\overline{\tau_g} = 2\varepsilon_g \mu_g \overline{D_g} + \varepsilon_g \lambda_g tr(\overline{D_g}) \overline{I}$$
 (20)

Where I is the identity tensor and Dg is the strain rate tensor for the fluid phase, given by:

$$\overline{D_g} = \frac{1}{2} \left[ \nabla \overrightarrow{V_g} + (\nabla \overrightarrow{V_g})^T \right]$$
 (21)

#### 2.3.4 Solids-Phase Stress Tensor

The theories are combined by introducing a "switch" at a critical packing,  $\varepsilon_g$ , the packed-bed void fraction at which a granular flow regime transition is assumed to occur:

$$\overline{S}_{sm} = -\begin{cases} -P_{sm}^{p} \overline{I} + \overline{\tau}_{sm}^{p} & if \quad \varepsilon_{g} \leq \varepsilon_{g}^{*} \\ -P_{sm}^{v} \overline{I} + \overline{\tau}_{sm}^{V} & if \quad \varepsilon_{g} > \varepsilon_{g}^{*} \end{cases}$$
(22)

th

Where  $P_{sm}$  is the pressure and is the viscous stress in the m solids phase. The superscript p stands for plastic regime and v for viscous regime. In fluidized-bed simulations,  $\epsilon_g$  is usually set to the void fraction at minimum fluidization. The granular pressure is given by:

$$P_{sm}^{V} = K_{lm} \varepsilon_{sm}^{2} \Theta_{m} \tag{23}$$

$$K_{lm} = 2(1 + e_{mm})\rho_{sm}g_{0mm} \tag{24}$$

The granular stress is given by

$$\overline{\tau}_{sm}^{V} = 2\mu_{sm}^{V} \overline{D}_{sm} + \lambda_{sm}^{V} tr(\overline{D}_{sm}) \overline{I}$$
 (25)

Where  $\lambda_{sm}^V$ , the second coefficient of viscosity for the  $m^{th}$  solids phase is given by:

$$\lambda_{sm}^{V} = K_{2m} \varepsilon_{sm} \sqrt{\Theta_m} \tag{26}$$

$$K_{2m} = \frac{4d_{pm}\rho_{sm}(1 + e_{mm})\varepsilon_{sm}g_{0_{mm}}}{3\sqrt{\pi}} - \frac{2}{3}K_{3m}$$
 (27)

$$=\frac{d_{pm}\rho_{sm}}{2}\left\{\frac{\sqrt{\pi}}{3(3-e_{mm})}[1+0.4(1+e_{mm})(3e_{mm})]\right\}$$

$$-1)\varepsilon_{sm}g_{0_{mm}}] + \frac{8\varepsilon_{sm}g_{0_{mm}}(1 + e_{mm})}{5\sqrt{\pi}}$$
 (28)

The factor  $\mu_{sm}^V$ , the shear viscosity for the  $m^{th}$  solids phase is

$$\mu_{sm}^{V}K_{3m}\varepsilon_{sm}\sqrt{\Theta_{m}}\tag{29}$$

The strain rate tensor,  $\overline{D_{sm}}$  is given by

$$\overline{D_{sm}} = \frac{1}{2} \left[ \nabla \overrightarrow{V_{sm}} + (\nabla \overrightarrow{V_{sm}})^T \right]$$
 (30)

Similar to the functions typically used in plastic flow theories (25), an arbitrary function that allows a certain amount of compressibility in the solids phase represents the solids pressure term for plastic flow regime:

$$P_{sm}^p = \varepsilon_{sm} P^* \tag{31}$$

Where  $P^*$  is represented by an empirical power law

$$P^* = A(\varepsilon_q^* - \varepsilon_q)^n \tag{32}$$

Typically, values of A=1025 and n=10 have been used. These stresses are calculated only for solids phase-1, even when multiple solids phases are specified:

$$\overline{\tau}_{sl}^p = 2\mu_{sl}^p \overline{D}_{sl} \qquad where \qquad \mu_{sl}^p = \frac{P^* \sin \varphi}{2\sqrt{I_{2D}}}$$
 (33)

The second invariant of the deviator of the strain rate tensor is

$$I_{2D} = \frac{1}{6} [(D_{s11} - D_{s22})^2 + (D_{s22} - D_{s33})^2 + (D_{s33} - D_{s11})^2] + D_{s12}^2 + D_{s23}^2 + D_{s31}^2$$
(34)

#### 2.4 Turbulence model

The effects of turbulent fluctuations of velocities and scalar quantities in the gas phase are described using the dispersed turbulence model. In this turbulence closure model, turbulence predictions for the continuous phase are obtained using the standard k-epsilon model(26) supplemented with extra terms dealing with interphase turbulent momentum transfer while predictions of the turbulence quantities for the particulate phase are obtained using the Techen-theory correlations.

#### 2.5 Turbulence in the continuous phase

The Reynolds stress tensor for the continuous phase takes the following form:

$$\overline{\tau_g} = -\frac{2}{3} \left( \rho_g \alpha_g k_g + \rho_g \alpha_g \mu_g^t \nabla \cdot \overrightarrow{V}_g \right) \overline{I} + 2 \rho_g \alpha_g \mu_g^t \overline{D}_g \qquad (35)$$

The turbulence viscosity  $\mu_q^t$  is written in terms of the turbulent kinetic energy of gas phase as:

$$\mu_g^t = \rho_g C_\mu \frac{k^2}{\varepsilon^g} \tag{36}$$

Where  $\varepsilon_q$  is the turbulence dissipation rate and  $C_{\mu} = 0.09$ . Turbulence predications of continuous phase are obtained from the following equations of modified k-epsilon model:

$$\frac{\partial}{\partial t} \left( \alpha_g \rho_g k_g \right) + \nabla \bullet \left( \alpha_g \rho_g \overrightarrow{V}_g k_g \right) = \nabla \bullet \left( \alpha_g \frac{\mu_g^t}{\sigma_k} \nabla k_g \right) + \alpha_g G_{k,g} + \prod_{kg} - \alpha_g \rho_g \varepsilon_g$$
 (37)

$$\frac{\partial}{\partial t} (\alpha_{g} \rho_{g} \varepsilon^{g}) + \nabla \bullet (\alpha_{g} \rho_{g} \overrightarrow{V}_{g} \varepsilon_{g})$$

$$= \nabla \bullet (\alpha_{g} \frac{\mu_{g}^{t}}{\sigma_{\varepsilon}} \nabla \varepsilon_{g})$$

$$+ \alpha_{g} \frac{\varepsilon_{g}}{k_{g}} (C_{1\varepsilon} G_{k,g} - C_{2\varepsilon} \rho_{g} \varepsilon_{g})$$

$$+ \prod_{\varepsilon_{g}} (38)$$

The influences of the dispersed phase on the continuous phase are given by:

$$\prod_{kg} = \beta \left( k_{gms} - 2k_g \right) \tag{39}$$

$$\prod_{\varepsilon g} = C_{3\varepsilon} \left( \frac{\varepsilon_g}{k_g} \right) \prod_{kg} \tag{40}$$

$$k_{gms} = \frac{\eta_t}{1 + (1 + X_{msg})\eta_t} (2k_g + 3X_{msg}\Theta_{ms})$$
 (41)

The production of turbulence kinetic energy, Gk,g, is computed

$$G_{k,g} = \mu_g^t \left( \nabla \overrightarrow{V}_g + (\nabla \overrightarrow{V}_g)^T \right) : \nabla \overrightarrow{V}_g$$
 (42)

### 2.6 Turbulence in the dispersed phase

Predictions for the turbulence quantities of the dispersed phase are obtained using the Tchen theory of dispersion of discrete particles by homogeneous turbulence (27, 28). The turbulence quantities include:

$$k_{ms} = k_g \left( \frac{b^2 + \eta_{sg}}{1 + \eta_{sg}} \right) \tag{43}$$

$$k_{sg} = 2k_g \left(\frac{b + \eta_{sg}}{1 + \eta_{sg}}\right) \tag{44}$$

$$D_{t,sg} = \frac{1}{2} k_{sg} \tau_{t,sg} \tag{45}$$

$$D_s = D_{t,sg} + \left(\frac{2}{3}k_{ms} - b\frac{1}{3}k_{sg}\right)\tau_{F,sg}$$
 (46)

$$= (1 + C_V) \left( \frac{\rho_{ms}}{\rho_g} + C_V \right)^{-1} \tag{47}$$

Where C<sub>V</sub> is the added-mass coefficient, equal to 0.5. and  $\tau_{F,sg}$  is the characteristic particle relaxation time connected with inertial effects acting on a dispersed phase.  $\tau_{t,sq}$  is the Lagrangian integral time scale calculated along particle trajectories.

#### 2.7 Aggregation, breakage and growth

In order to account for the particle size distribution (PSD), a population balance must be solved simultaneously with the other equations(29). In this work, the direct quadrature method of moments (DQMOM) is combined with the multifluid CFD model to describe polydisperse solids undergoing aggregation, breakage, and growth. The detailed derivation of the DQMOM equations is given by Fan (30). Neglecting changes in momentum due to aggregation and breakage, the DQMOM equations are:

$$\frac{\partial \varepsilon_g \rho_g}{\partial t} + \nabla \cdot \left( \varepsilon_g \rho_g u_g \right) = -\sum_{m=1}^{N_{sm}} 3k_v \rho_s d_{pm}^2 \omega_m G_m \tag{48}$$

$$\frac{\partial \varepsilon_{sm} \rho_{sm}}{\partial t} + \nabla \cdot (\varepsilon_{sm} \rho_{sm} u_{sm}) = 3k_v \rho_{sm} d_{pm}^2 (b_m + \omega_m G_m) - 2k_v \rho_{sm} d_{pm}^3 a_m$$

$$(49)$$

$$\begin{split} &\frac{\partial \varepsilon_{sm} \rho_{sm} d_{pm}}{\partial t} + \nabla \cdot \left( \varepsilon_{sm} \rho_{sm} d_{pm} u_{sm} \right) \\ &= 4 k_{\nu} \rho_{sm} d_{pm}^{3} (b_{m} + \omega_{m} G_{m}) \\ &- 3 k_{\nu} \rho_{sm} d_{pm}^{4} a_{m} \end{split} \tag{50}$$

Where the particle number density  $\omega_m$  is related to the solids volume fraction by

$$\omega_m = \frac{\varepsilon_{sm}}{k_v d_{nm}^3} \tag{51}$$

The shape factor  $k_{\nu}$  depends on the particle morphology and has a value for  $k_{\nu}=\pi/6$  for spherical particles. The rates of aggregation and breakage determine the rate constants  $a_m$  and  $b_m$ .

### 2.8 Equation of state and other equations

The fluid phase can be modeled as a gas obeying the ideal gas law,

$$\rho_g = \frac{P_g M_w}{R T_g} \tag{52}$$

Or as an incompressible fluid with a constant density. The user may specify any other equation of state by modifying the equation of state subroutine (EOSG). These volume fractions are assumed to be continuous functions of space and time. By definition, the volume fractions of all of the phases must sum to one:

$$\varepsilon_g + \sum_{m=1}^M \varepsilon_{sm} = 1 \tag{53}$$

Where M is the total number of solids phases

#### 3 Results and discussion

The two dimensional model is considered with width and height of 5 and 30 cm, respectively. The properties of solid and gas are shown in Table 1. This calculating area was discreet to 20\*90 cells and the time of modeling (physical time) was considered 10 sec. The following assumptions were made for the simulations.

- Physical properties such as temperature, density and viscosity of the gas and solid are assumed to be constant.
- 2) Mass transfer between solid phases is ignored.
- 3) The gas phase is composed of pure air.
- 4) Two solid phases with different initial diameters and volume fractions are used to represent aggregation and breakage.
- The aggregation and breakage efficiencies are independent of particle size.

In the present study, by designing optimum gas distributor, it is tried to reduce the required time for lump formation in the polymerization reactor. Accordingly, three types of gas distributor with different spacing in inlet vents were considered and the results were investigated in three case studies. Figure 1 shows the features of gas distributor in lower section of the polymerization reactor. It is obvious that difference in inlet vents spacing is a function of fluidized bed reactor. But the sectional velocities of all distributors were equal to 0.25 m/s (see Table 1). Gas velocity in inlet vents of distributors for case studies 1 to 3 are 0.25, 0.535 and 1.25 m/s, respectively.

Table 1: The CFD domain and parameters used in the simulation

Property	units	value
Number of phases of solid particles, N	-	2
Initial diameter of particles, $d_{pm}$	μm	408 & 168
Density, $\rho_{\rm ms}$	$Kg/m^3$	2530
Friction factor, e	-	0.8
Internal friction angle, φ	degree	30.0
rate of particle attachment	-	0.001
Particle breaking rate	-	0.0001
Hold up of compact bed, $\varepsilon_g^*$	-	0.48
Reactor pressure	atm	20
Inlet gas temperature	K	316
Gas density, pg	Kg/m3	0.1
Gas viscosity, µg	Pa.s	0.0000114
Average velocity of inlet gas on the cross-platform, U	m/s	0.25

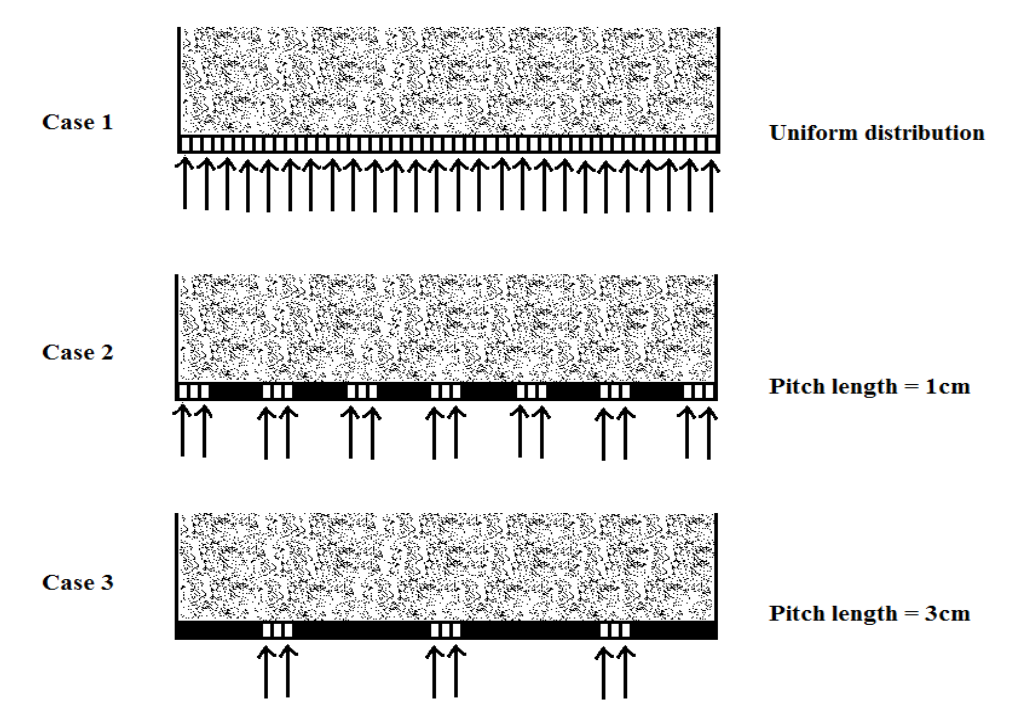


Figure 1: Schematic of the gas distributor for the three case studies

#### 3.1 Distribution of gas hold-up

Contours of gas hold-up in different times and for all three gas distributors are shown in Figures (2) to (4). Because of high rate of particle attachments inside the reactors compared with particle cracking, the number of particles inside fluidized bed reactor increases. The sectional fluidizing velocity is constant for all case studies; therefore, as the velocity of particles decreases in these beds the size of bubbles increases until the beds velocity move toward zero. The conditions in which fluidizing disappears inside the reactors are shown in Figures 2 to 4. As it is seen in these figures, as time increases gravity force will also increase due to enlargement of size and mass of particles and drag force cannot move the particles to a higher height. Since particle diameter increases, the height of bed decreases (reduction in bed expansion) and finally the bed Figures (2) to (4) show that loses the fluidizing state. fluidizing state of distributors with bigger spacing happens later and fluid bed with steady gas distributor loses fluid state

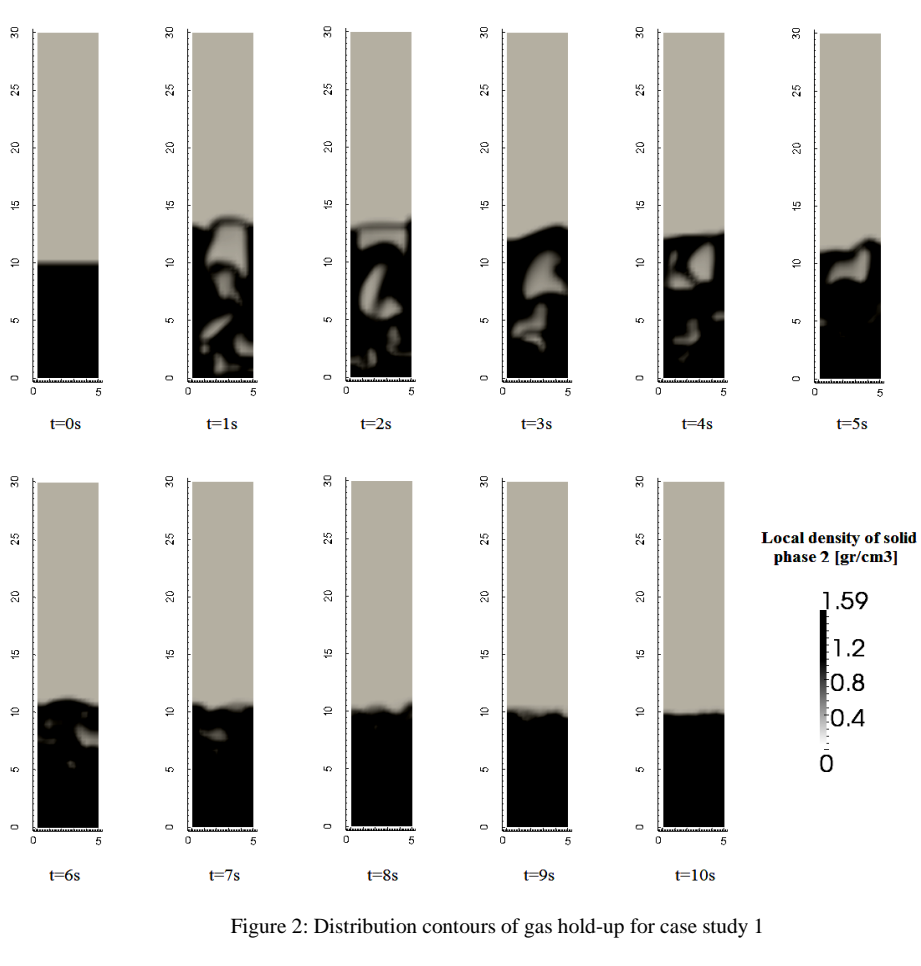
## 3.2 Distribution of apparent density and mass fraction of particles

According to time delay applied for preventing flocculation and fluidizing state in previous section, selection of gas distributor with larger spacing would be a better choice. But uncontrolled conditions and tendency to flocculation happen in fluidized bed reactors. Two points should be considered in these reactors:

 Gas distribution in fluid bed for longer contact time of gas phase (reaction monomers) for optional stay time in reactors; Reactor recovery as a result of a decrease in the produced number of polymer particles which should be in desired level (a market grade with appropriate standards);

The more steady gas distribution inside the bed, the more suitable stay time and gas contact with active solid particles (with active continuum for reaction with gas monomer). A good indicator of this point is the expansion of fluid bed or average volume fraction of gas for initial moments of fluidizing just before critical state and bed alleviation. Accordingly, the bed of gas distributor with larger spacing is not suitable for continuous reactor polymerization.

In order to investigate the distribution of apparent density and mass fraction of fine and coarse particles inside the case studies, Figures (6) to (8) obtained from numerical modeling will be discussed. Considering the contours shown for coarse particles, the accumulation of these particles in the lower section of fluidized beds was observed; meaning that coarse particle separation happens in the lower section and transfer of fine solid particles will be toward upper fluidized beds(31). As time increases and enhancement occurs in fluidized alleviation, in all three case studies decrease in the size of gas bubbles in the lower section up to the free surface of beds was observed. Designing fluidized bed applicable polymerization reactors, discharge of produced powder takes place from the lower section of the bed. As a result, the diameter increases and accumulates in the lower section of the bed leading to flocculation and shutting gas inlet. Regarding Figures (6) to (8), a gas distributor with larger spacing has a better function for prevention of coarse particle accumulation on the gas distributor.



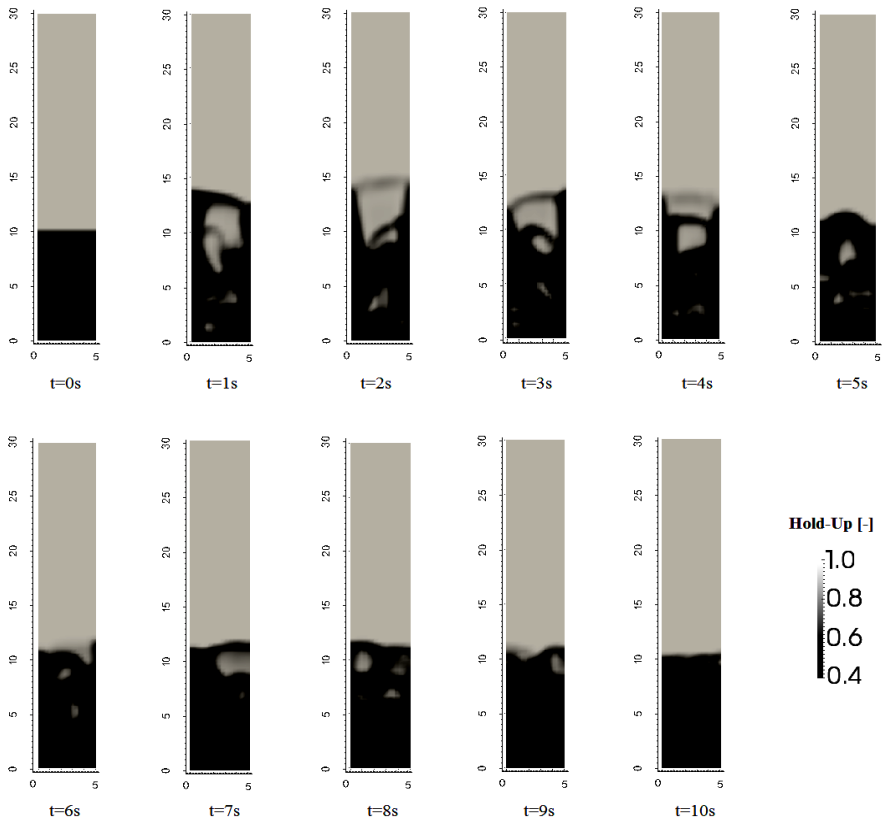


Figure 3: Distribution contours of gas hold-up for case study 2

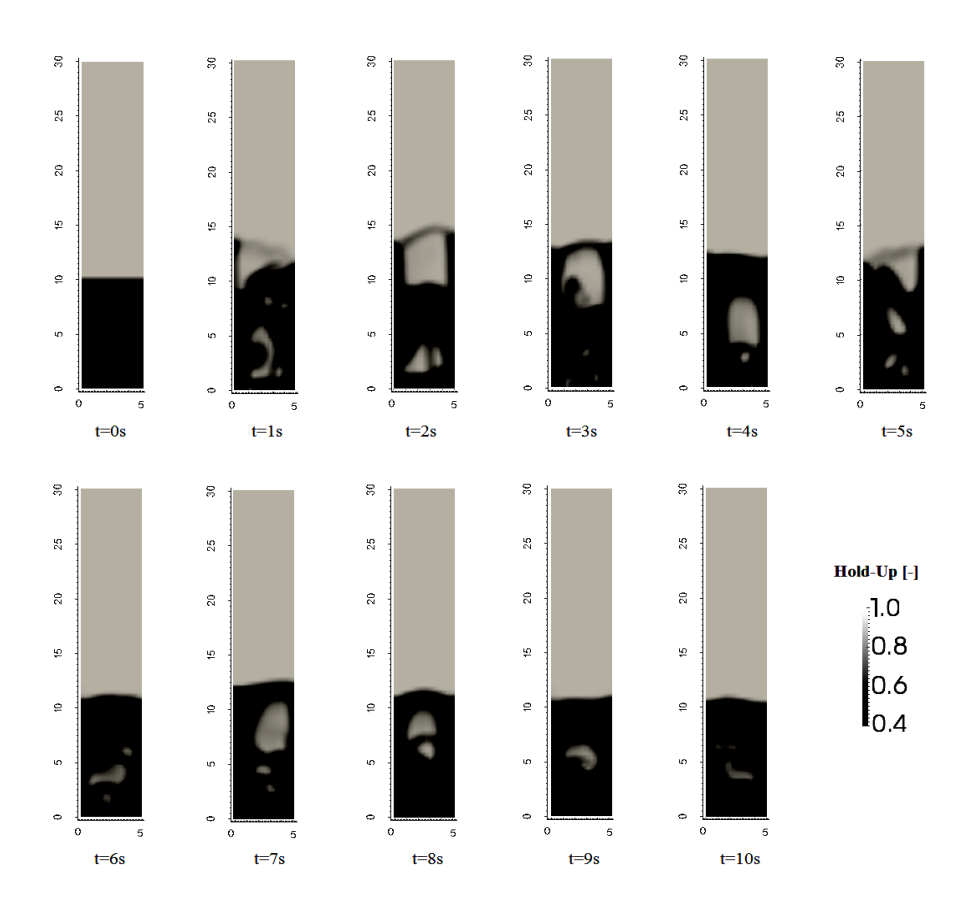


Figure 4: Distribution contours of gas hold-up for case study 3

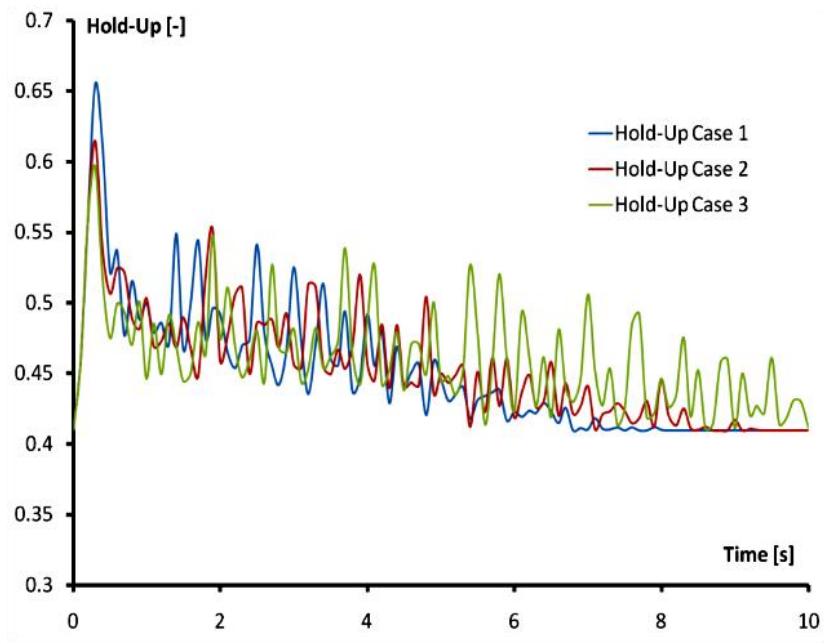


Figure 5: Average spatial distribution of gas hold-up in the fluidized bed versus time for three type of different gas distributors

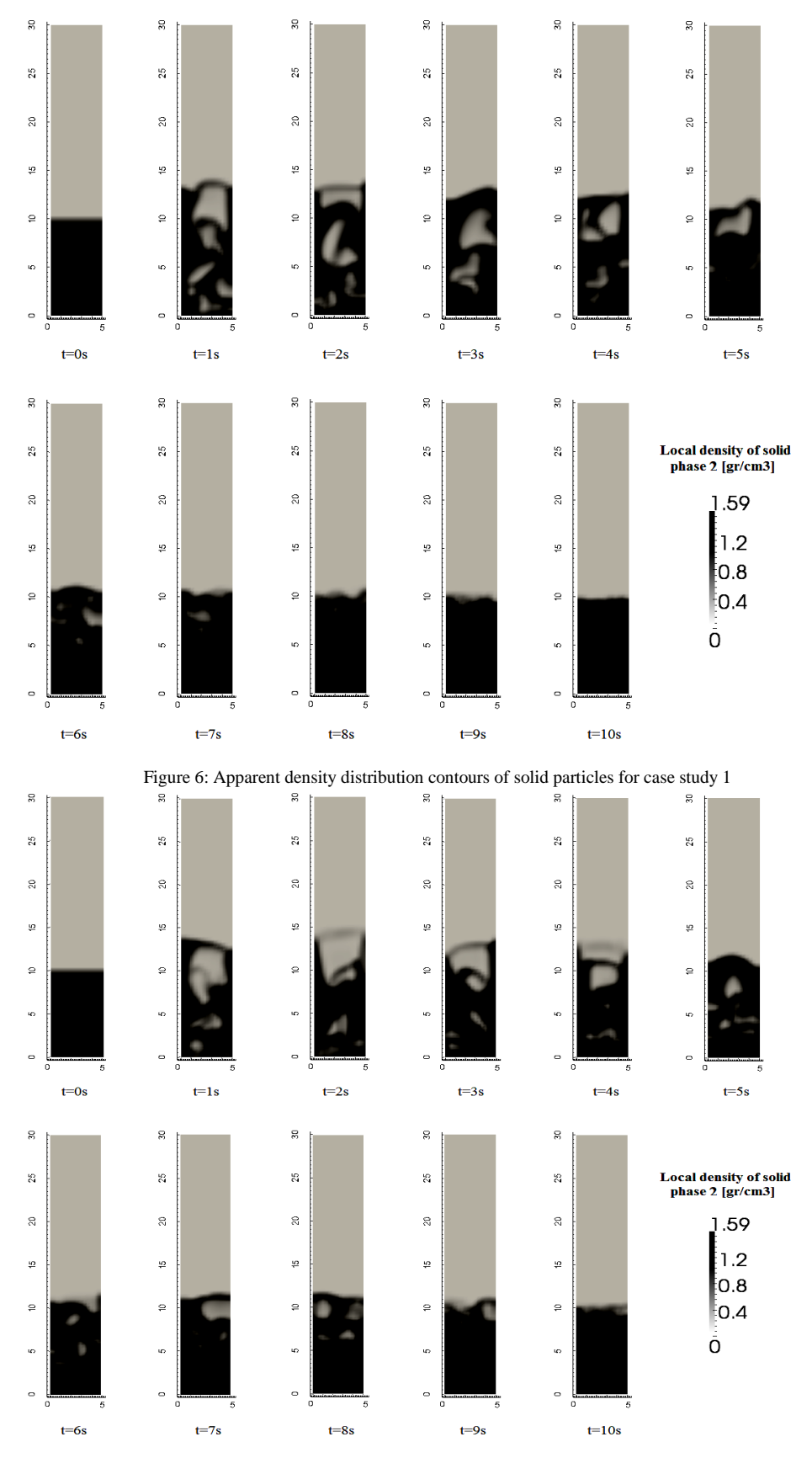


Figure 7: Apparent density distribution contours of solid particles for case study 2

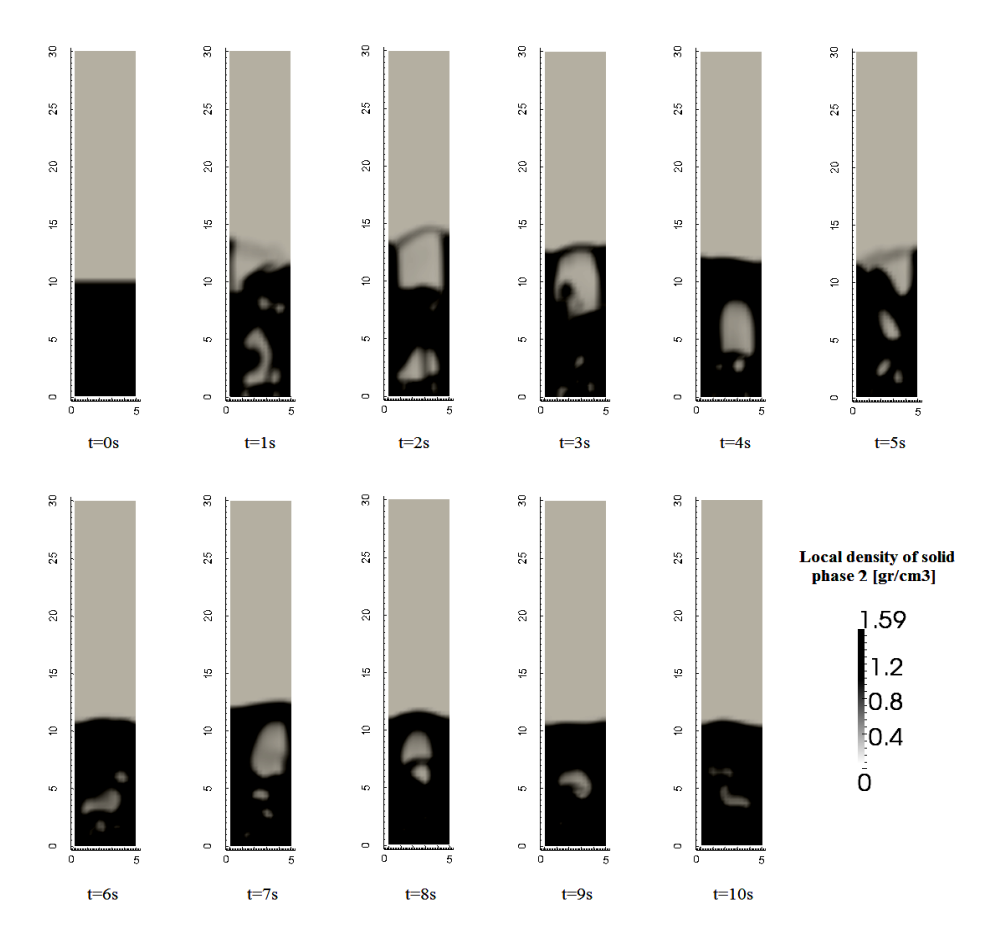


Figure 8: Apparent density distribution contours of solid particles for case study 3

#### 3.3 Particle Size Distribution

Particle size distribution is affected by two factors: 1) particle attachment; 2) physical and chemical cracking of particles(32). In fluidized bed reactors, one of the physical factors is particle collision. In lower temperatures the possibility of cracking in particles increases and otherwise, the possibility of flocculation increases. On the other hand, reaction with monomer increases the size of particles and in case of cohesion presence in the system (polymer eutectic) the number of coarse particles increases.

Studies on chemical effects need an investigation of catalysts and operational conditions in the reactor. But physical factors depend on flow regime and reactor designing parameters like a gas distributor. In the present study, the size distribution of a poly-ethylene polymerization reactor was calculated using numerical modeling for a typical reactor in normal conditions. In other words, some parameters considered constant including growth rate, solid particle cracking from chemical reactions, particle cohesion and particle cracking due to the physical collision of powder particles. The only variable was the difference in gas and solid distribution which is produced by different gas distributors. In Figure (9), the changes in the number of fine particles (averaged with inside volume of reactor) versus time is shown. As it is seen, the number of particles increases as time passes. In addition, the diameter of fine particles for the steady gas distributor is larger and for long spacing gas distributor is shorter.

In Figure (10) the average diameter of coarse particles versus time is shown similar to Figure (9) and the different trend is observed for these particles. In the beginning, with similar initial conditions, the diameter of coarse particles increases and the difference between size distributions in the

beds versus time is observed. But this difference is not significant between the steady gas distributor and medium spacing gas distributor. As time passes, increase in the number of coarse particles on the beds with steady distributor stops 6 seconds after fluidizing which is a function of fluidized alleviation and settling coarse particles. This time is equal to 8 seconds for the medium spacing gas distributor. On the third bed the diameter of coarser particles increases which implies fluidizing behavior.

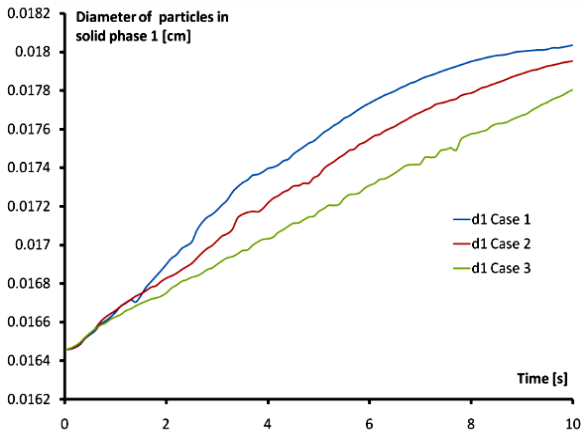


Figure 9: Average size of the fine solid particles (first step of solid particles) versus time for different gas distributors

In order to determine the average number of fine and coarse particles inside the fluidized bed, it should be determined the mass percentage of fine and coarse particles. In Figure (11), modeling time distribution of fine solid particles for different gas distributors is shown. It is obvious that mass fraction of coarse particles is equal to unity minus this value which is shown in Figure (12).

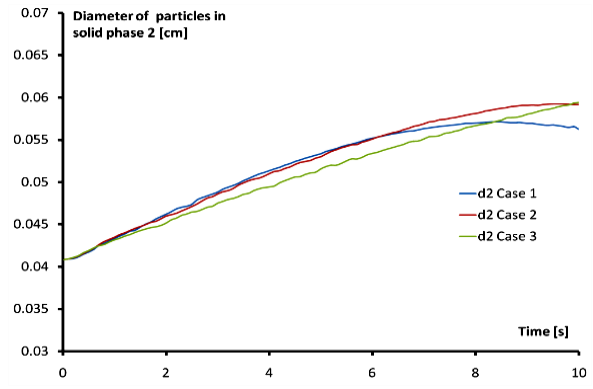


Figure 10: Average size of the coarse solid particles (second step of solid particles) versus time for different gas distributors

Mass fraction of coarser particles increases with time and mass fraction of finer particles decreases. According to the results, it is clear that mass fraction of coarser particles for gas distributors with larger spacing is less than other distributors. More fine particles attend inside the bed. Although it is a negligible amount, it promotes to a larger extend to fluidizing and delay in the alleviation of the bed.

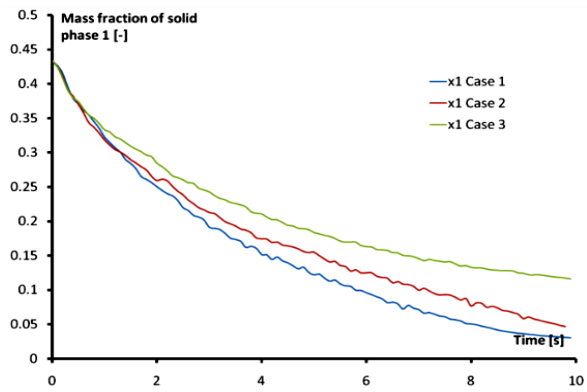


Figure 11: The average of the fine solid particles hold-up (first step) versus time for different gas distributors

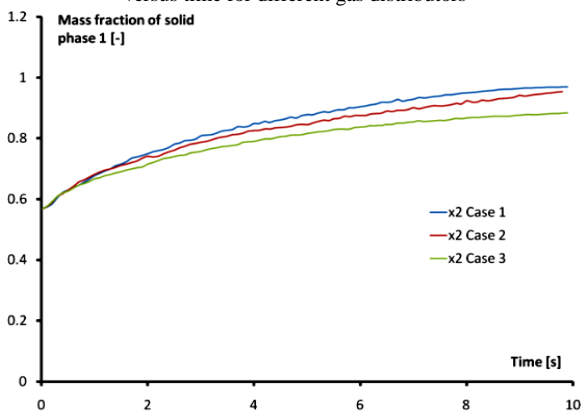


Figure 12: The average of the coarse solid particles hold-up (second step) versus time for different gas distributors

Figure (13) shows the average particle diameter inside the fluidized beds for different distributors that is produced by merging Figures (10) to (12). This figure shows that increasing unsteadiness in the gas distributor inlets decreases

the average diameter of the particles. This result is due to changes in flow regime and convection term (Equations (155) to (161)) inside fluidized reactors.

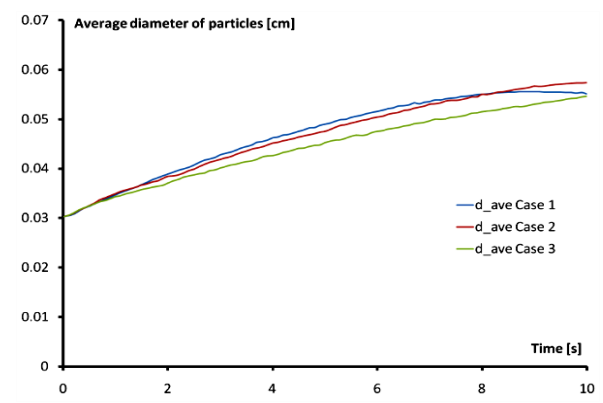


Figure 13: The average size of solid particles (Average of first and second steps of solid particles) versus time for different gas distributors.

#### 4 Conclusions

A detailed CFD model for sticky poly propylene fluidized bed was formulated in this work. As a result, detailed information on the PSD and hydrodynamic fields of the gas and solid phases can be obtained from the simulations. Defluidization due to particle aggregation also can be simulated. For modeling plant-scale poly propylene reactors, a chemical look-up table should be used to solve efficiently the solid species equations. The aggregation and breakage efficiencies should also be related to the particle velocity and As a result, physically aggregation xylem solubility. because of atactic polypropylene is more important than other aggregation reasons. Finally, as mentioned earlier, after DQMOM is applied to the multi-fluid CFD model, new terms accounting for the effect of aggregation and breakage need to be added on the right-hand sides of the solid-phase momentum, energy, and species equations. modifications and detailed simulation results for plant-scale fluidized bed polymerization reactors will be reported in future communications. During simulation, the growth rate of the number of particles has a good match with gas distribution in the fluidized bed. Increasing mass and particle size, gravity force increases and drag force cannot move the particles to a higher height. On the other hand, for the larger diameter of the particles, the height of the bed decreases (reduction in the expansion of the bed) and finally the bed lose its fluidizing state. If solid particles were not expelled from the reactor in a definite time or an unpredictable growth takes place, primary conditions for formation of flocculation would be provided and as a result the whole reactor would be filled with melted polymer and after shutting down, a polymer cast would be created that needs about six months for cleaning and discharge. Obviously, significant losses would be created and this confirms the importance of this study for optimization. According to the results, more steady gas flow in the gas distributors of polymer fluidized beds, the higher will be the growth rate. But for sharper gas distribution (longer spacing between the gas inlets), the fluidizing state of the bed tends to flocculation later. Therefore, an optimized option should be considered for a gas distributor in designing polymerized reactor. It is suggested that a steady gas distributor should be selected for fluidized bed and this is done by dividing distributor area into a number of sections and inlet gas is designed into the reactor with tree diagram pattern. In case of all open inlets, the flow would be steady and in case of some closed inlets, the spacing between inlets will increase. Such flexibility leads to the suitable function of the normal reactor and prevents flocculation in critical conditions. As a result, without fundamental changes in polymerized reactor structure that costs a huge amount, optimization would be performed.

#### References

- Fan L-S, Zhu C. Principles of gas-solid flows: Cambridge University Press; 2005.
- Mousavi S, Arjmand O, Talaghat M, Azizi M, Shooli H. Modifying the properties of polypropylene-wood composite by natural polymers and eggshell Nano-particles. Polymers from Renewable Resources. 2015;6(4):157-73.
- Goudarzian N, Saleh R, Mousavi S. Recovery of Poly Ethylene Amine Nano Cerium Methoxy Bohrohydride Reagent: A New Class of Polymeric Reducing Agent. Int J Chem Sci. 2018;16(3):271.
- Yiannoulakis H, Yiagopoulos A, Kiparissides C. Recent developments in the particle size distribution modeling of fluidized-bed olefin polymerization reactors. Chemical Engineering Science. 2001;56(3):917-25.
- Szafran RG, Kmiec A. CFD modeling of heat and mass transfer in a spouted bed dryer. Industrial & engineering chemistry research. 2004;43(4):1113-24.
- Goudarzian N, Hashemi SA, Mirjalili M. Unsaturated polyester resins modified with cresol novolac epoxy and silica nanoparticles: processing and mechanical properties. International Journal of Chemical and Petroleum Sciences. 2016;5(1):13-26.
- Armaghani T, Esmaeili H, Mohammadpoor Y, Pop I. MHD mixed convection flow and heat transfer in an open C-shaped enclosure using water-copper oxide nanofluid. Heat and Mass Transfer. 2018;54(6):1791-801.
- Esmaeili H, Armaghani T, Abedini A, Pop I. Turbulent combined forced and natural convection of nanofluid in a 3D rectangular channel using two-phase model approach. Journal of Thermal Analysis and Calorimetry. 2019;135(6):3247-57.
- Lun C, Savage SB, Jeffrey D, Chepurniy N. Kinetic theories for granular flow: inelastic particles in Couette flow and slightly inelastic particles in a general flowfield. Journal of fluid mechanics. 1984;140:223-56.
- Syamlal M. The particle-particle drag term in a multiparticle model of fluidization. EG and G Washington Analytical Services Center, Inc., Morgantown, WV (USA); 1987.
- Syamlal M. A review of granular stress constitutive relations. EG and G Washington Analytical Services Center, Inc., Morgantown, WV (USA); 1987.
- Mousavi SM, Hashemi SA, Babapoor A, Medi B. Enhancement of Rheological and Mechanical Properties of Bitumen by Polythiophene Doped with Nano Fe 3 O 4. JOM. 2019;71(2):531-40.
- Syamlal M, O'Brien T. A generalized drag correlation for multiparticle systems. Unpublished report. 1987.
- Richardson J, Zaki W. Sedimentation and fluidisation: Part I. Chemical Engineering Research and Design. 1997;75:S82-S100.
- Garside J, Al-Dibouni MR. Velocity-voidage relationships for fluidization and sedimentation in solid-liquid systems. Industrial & engineering chemistry process design and development. 1977;16(2):206-14.
- Khan A, Richardson J. The resistance to motion of a solid sphere in a fluid. Chemical Engineering Communications. 1987;62(1-6):135-50.
- 17. DallaValle JM. Micromeritics: the technology of the particles: Pitman Publishing Corporation; 1943.
- Arastoopour H, Lin D, Gidaspow D. Hydrodynamic analysis of pneumatic transport of a mixture of two particle sizes. Multiphase Transport. 1980;4:1853-71.
- Arastoopour H, Wang C-H, Weil SA. Particle—particle interaction force in a dilute gas—solid system. Chemical Engineering Science. 1982;37(9):1379-86.
- Soo S-I. Fluid dynamics of multiphase systems. WALTHAM, MASS, BLAISDELL PUBLISHING CO, 1967 524 P, 206 FIG, 8 TAB, 886 REF. 1967.

- Capes C, Nakamura K. Vertical pneumatic conveying: an experimental study with particles in the intermediate and turbulent flow regimes. The Canadian Journal of Chemical Engineering. 1973;51(1):31-8.
- Syamlal M. Multiphase hydrodynamics of gas-solids flow: Illinois Institute of Technology; 1985.
- Srinivasan M, Doss E. Momentum transfer due to particle particle interaction in dilute gas—solid flows. Chemical engineering science. 1985;40(9):1791-2.
- Lebowitz J. Exact solution of generalized Percus-Yevick equation for a mixture of hard spheres. Physical Review. 1964:133(4A):A895.
- Jenike A. A theory of flow of particulate solids in converging and diverging channels based on a conical yield function. Powder technology. 1987;50(3):229-36.
- Arjmand O, Izadi S, Mousavi M, Rahmanian V. Polyvinyl alcohol with superior flooding properties to enhance oil recovery process. Research Journal of Applied Sciences, Engineering and Technology. 2012;4(17):3062-4.
- Hinze J. Turbulence. McGraw-Hill Publishing Co. New York; 1975
- 28. Mousavi SM, Hashemi SA, Amani AM, Saed H, Jahandideh S, Mojoudi F. Polyethylene terephthalate/acryl butadiene styrene copolymer incorporated with oak shell, potassium sorbate and egg shell nanoparticles for food packaging applications: control of bacteria growth, physical and mechanical properties. Polymers from Renewable Resources. 2017;8(4):177-96.
- Mousavi S, Aghili A, Hashemi S, Goudarzian N, Bakhoda Z, Baseri S. Improved morphology and properties of nanocomposites, linear low density polyethylene, ethylene-covinyl acetate and nano clay particles by electron beam. Polymers from Renewable Resources. 2016;7(4):135-53.
- Fan R, Marchisio DL, Fox RO. Application of the direct quadrature method of moments to polydisperse gas-solid fluidized beds. Powder technology. 2004;139(1):7-20.
- 31. Mousavi SM, Hashemi SA, Jahandideh S, Baseri S, Zarei M, Azadi S. Modification of phenol novolac epoxy resin and unsaturated polyester using sasobit and silica nanoparticles. Polymers from Renewable Resources. 2017;8(3):117-32.
- 32. Hashemi SA, Mousavi SM. Effect of bubble based degradation on the physical properties of Single Wall Carbon Nanotube/Epoxy Resin composite and new approach in bubbles reduction. Composites Part A: Applied Science and Manufacturing. 2016;90:457-69.